Characterization of Polydisperse Solutions of Branched Poly(methyl methacrylate) Using Size Exclusion Chromatography with On-Line Multiangle Light Scattering and Viscosity Detection

Christophe Degoulet, Taco Nicolai,* Dominique Durand, and Jean Pierre Busnel

Laboratoire de Physico-Chimie Macromoléculaire, CNRS URA 509, Université du Maine BP 535, 72017 Le Mans Cedex, France

Received October 24, 1994; Revised Manuscript Received May 11, 1995[⊗]

ABSTRACT: We have studied the mass distribution ($N(M)$) of branched poly(methyl methacrylate) (PMMA) formed by radical copolymerization of methyl methacrylate and ethylene glycol dimethacrylate by size exclusion chromatography (SEC). We show how the static structure factor of monodisperse branched PMMA can be obtained using a new type of on-line multiangle light scattering detector. We compare the monodisperse static structure factor with that of the polydisperse solutions and show that the polydisperse static structure factor can be derived from the monodisperse function using $N(M)$ obtained from SEC. Both the static structure factor and the mass distribution are found to be consistent with predictions from percolation theory. Using an on-line viscometer we have determined the molar mass dependence of the intrinsic viscosity.

Introduction

Broad distributions of branched macromolecules are obtained by many different types of aggregation processes or (co)polymerization of polyfunctional monomers; see for example refs 1–9. The average particle size increases with increasing reaction extent, and the process might eventually lead to the formation of a gel. In order to understand the aggregation or polymerization process, it is necessary to determine the structure and the mass distribution of the particles. In the case of gel formation, an analysis of the pregel solutions may help to understand the properties of the gel.

The structure of large, but still microscopic, particles can be studied most easily by scattering techniques, while size exclusion chromatography (SEC) allows one to study the size distribution. SEC combined with one-line light scattering detection seems therefore very promising for the analysis of polydisperse distributions. A number of studies of such systems with light scattering detection at a single small scattering angle have been reported.[7–9] We have recently developed a multiangle light scattering (MALS) detector which allows an on-line determination of the static structure factor. Unfortunately, using light scattering the static structure factor of the particles (S) can only be determined over a limited range of the scattering wave vector ($q = (4\pi n/\lambda)\sin(\theta/2)$, with n the refractive index of the solution, λ the wavelength of the incident light, and θ the angle of observation). However, particles of different size formed by the same aggregation or polymerization process are often self-similar; i.e., they have a fractal structure.[10,11] The fractal structure implies that S is independent of the size of the particles if plotted as a function of qR_g, where R_g is the radius of gyration of the particles. If one uses this feature, S can be obtained over a wide q-range by combining measurements on different size particles in the same solution.

Here we apply this method to the analysis of polydisperse solutions of branched poly(methyl methacrylate) (PMMA) formed by copolymerization of methyl methacrylate (MMA) and ethylene glycol dimethacrylate (EGDMA) in solution. This copolymerization leads to the formation of a transparent gel at reaction extents that depend on the MMA concentration and the molar ratio [MMA]/[EGDMA]. After a brief outline of the theory of light scattering by self-similar particles, we present the results obtained by SEC with combined refractive index (RI), MALS, and viscosity detection. We show how the static structure factor and the mass distribution can be determined and how the static structure factor is influenced by polydispersity. We compare these results with predictions from percolation theory.[12] We find that if one applies the so-called universal calibration[13] to branched PMMA, the molar mass is about 25% smaller than the values obtained from light scattering measurements.

Light Scattering Theory

The intensity of the light scattered by dilute solutions of monodisperse noninteracting particles with molar mass M is[14,15]

$$I = kMCS \tag{1}$$

where C is the particle concentration in weight per volume and k is a constant which depends on the experimental setup, the refractive index increment of the solution, and the wavelength of the incident light in the solution. In general, S depends in a complicated way on the detailed structure of the particles, but in the so-called Guinier regime where $qR_g < 1$, S can be written as a series development in $(qR_g)^2$

$$S = 1 - \frac{1}{3}(qR_g)^2 + \ldots \tag{2}$$

For fractal systems the static structure factor as a function of qR_g is independent of R_g for $qr_0 \ll 1$. In the limit of large qR_g, it can be shown that[16]

$$S(qR_g) \propto (qR_g)^{d_f} \qquad qR_g \gg 1 \text{ and } qr_0 < 1 \tag{3a}$$

and

[⊗] Abstract published in *Advance ACS Abstracts,* August 1, 1995.

0024-9297/95/2228-6819$09.00/0

$$M \propto R_g^{d_f} \qquad R_g \gg r_0 \tag{3b}$$

where d_f is the fractal dimension and r_0 is the internal cutoff of the fractal regime. The shape of $S(qR_g)$ around $qR_g = 1$ depends on the surface structure of the particle.

For polydisperse solution we need to sum the contributions of particles with different size so that

$$I(q) = k\sum(M^2N(M)S(M,q)) \tag{4}$$

where $S(M,q)$ is the static structure factor of particles with molar mass M. $N(M)$ is the number concentration of particles with molar mass M normalized such that

$$\sum MN(M) = C \tag{5}$$

Equations 2 and 3 remain valid for polydisperse solutions if we replace R_g by the square root of the z-average squared radius of gyration (R_{gz}) and M by the weight-average molar mass (M_w). Often in the case of aggregation or polymerization of multifunctional monomers, the mass distribution is expected to have the following shape:[10,11]

$$N(M) \propto M^{-\tau} f(M/M^*) \qquad M > M_0 \tag{6}$$

where M_0 is the mass of the smallest particle of the distribution and $f(M/M^*)$ is a cutoff function at a characteristic mass M^*, which decreases faster than any power law. Polydispersity has a strong influence on the q-dependence of I, but only affects the limiting behavior at large q if $\tau > 2$. In the latter case, the limiting slope of $\log(I)$ versus $\log(q)$ is given by $d_{f,pol} = d_f(3 - \tau)$ retaining, of course, the condition $qr_0 < 1$. A detailed discussion of the influence of the surface structure and the polydispersity of fractal particles on the q-dependence of I is given elsewhere.[17]

Experimental Section

Materials. The samples were prepared by radical copolymerization of 0.235 g·cm^{-3} MMA and EGDMA in toluene using 1.1×10^{-3} g·cm^{-3} AIBN to initiate the reaction. The molar ratio [EGDMA]/[MMA] was 0.01. The solutions were filtered through 0.2 μm Anatop filters after which the polymerization occurred in a thermostated bath at 68 ± 0.1 °C under continuous agitation. At set time intervals a sample was rapidly cooled in an ice bath in order to quench the reaction. The samples were diluted in THF for SEC and LS analysis with a small amount of inhibitor added to prevent further polymerization. For this study we used eight samples quenched at different reaction extents R, defined as the fraction of MMA that has reacted to form branched PMMA (see Table 1).

Experimental Setup. We used a classical analytical SEC apparatus coupled to a multiangle light scattering and viscosity detector which has recently been developed in our laboratory.[18] Two PL-Gel columns (Polymer Laboratories, MIX-34-22 and MIX-B-72-8, each 600 × 7.5 mm, particle diameter 10 μm) were used in series. The eluant was THF and the flow rate 1 cm^3/min. The concentration was monitored by a differential refractometer (R410 from Millipore-Waters) using 0.09 for the refractive index increment of PMMA in THF. The light source for the light scattering detection is a He/Ne laser emitting light with wavelength 633 nm. Molar masses were calculated using 1.4×10^{-5} cm^{-1} for the Rayleigh ratio of a toluene standard. The scattered light intensity of discrete fractions of 1 cm^3 was measured simultaneously at 10 angles between 15 and 150°. The viscosity of each fraction was measured using a capillary viscometer thermostated at 20 °C. The measurement temperature was monitored within ±0.01 °C. The advantage of measuring discrete fractions over continuous detection is that more accurate values of the intensity are obtained and the viscosity measurements are not influenced by fluctuations in the flow rate. The error in the excess scattering intensity (I) is within ±1% of the scattered light intensity of pure THF (I_{THF}), while the error in the excess flow time (t) is measured within ±1 ms. Typical values of the maximum excess intensity and excess flow time for the systems studied here were about 5 × I_{THF} and 300 ms, respectively. The disadvantage of measuring discrete fractions is the reduced number of data points to characterize the distribution and the residual polydispersity of the fraction. However, for the size of the columns used in this study, the polydispersity introduced by the finite size of the fractions is small compared to the effect of band broadening. The amount of structural polydispersity, i.e., particles with the same hydrodynamic radius but different molar mass, is probably small due to the fractal nature of the particles. Typically 0.3 cm^3 solutions were injected with a concentration of about 1.5 × 10^{-3} g·cm^{-3}, leading to a maximum concentration in the fractions of 5 × 10^{-5} g·cm^{-3}, which means that second virial interactions can be neglected.

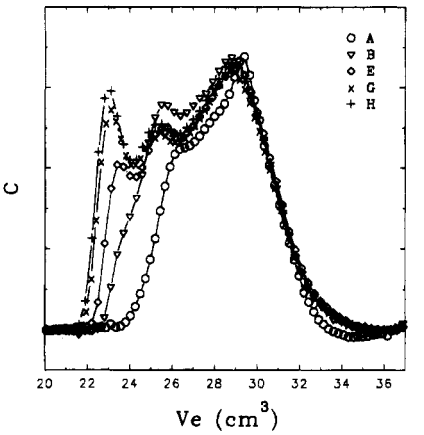

Figure 1. Refractive index signal as a function of the elution volume for five samples at different reaction extents (see Table 1).

Table 1. Sample Characteristics

sample	R	$M_{cal} \times 10^{-6}$ (g·mol^{-1})	$M_w \times 10^{-6}$ (g·mol^{-1})
A	0.16_1	1.0_6	0.8
B	0.19_0	1.6_6	1.3
C	0.19_0	1.9_2	2.1
D	0.20_3	2.2_6	2.9
E	0.21_7	2.8_0	5.5
F	0.21_7	2.4_2	>15
G	0.22_2	2.8_3	>15
H	0.23_0	2.7_8	>15

Results

Eight solutions of branched PMMA obtained by quenching the reaction at different reaction extents were analyzed by SEC using combined RI, MALS, and viscosity detection. In Figure 1 the RI signal is shown as a function of the elution volume (V_e). The toluene and residual monomers are eluted at $V_e \approx 43$ cm^3 and the corresponding peaks are not shown in Figure 1. In the initial stage of the reaction, mainly linear polymers are formed with weight-average molar mass $M_w \approx 70\,000$ g·mol^{-1} and $M_w/M_n \approx 2$. As the reaction continues, branched PMMA chains are formed of increasing size and the mass distribution broadens. It is noted that the maximum position of the distribution, which corresponds to the linear PMMA, does not move with increasing reaction extent. At later stages of the reaction, the largest particles are not separated but leave the column at approximately the same value of V_e. The reaction extents (R) are determined by inte-

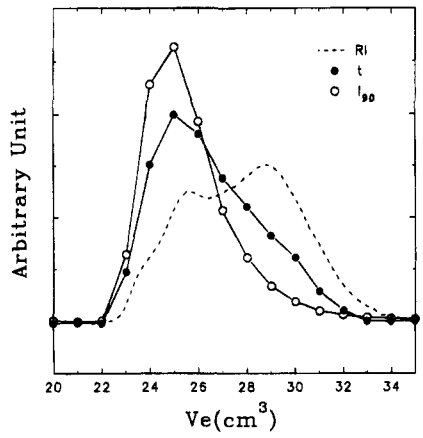

Figure 2. Comparison of the RI signal, the excess scattering intensity at $\theta = 90°$, and the excess flow time as a function of the elution volume for sample C. The curves have been normalized to given an equal surface area.

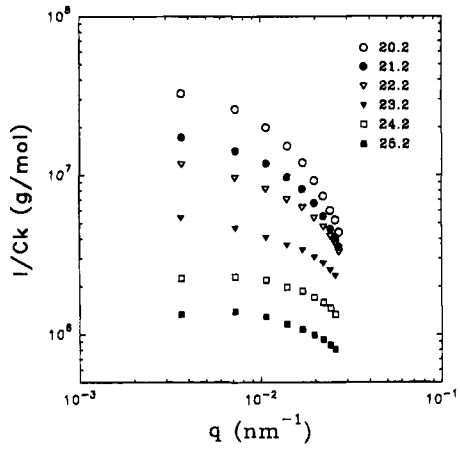

Figure 3. Double-logarithmic representation of the q-dependence of $I/(kC)$ of sample H at the different elution volumes indicated. $I/(kC) = M$ in the limit of $q = 0$.

grating the polymer peak area of the RI signals (see Table 1).

In Figure 2 the RI signal, the excess scattering intensity at $\theta = 90°$ (I_{90}), and the excess flow time t are shown as a function of V_e for sample C. If we assume that the interaction between the particles is negligible, RI, I_{90}, and t are related to the particle concentration in the following way:

$$\mathrm{RI} \propto C$$

$$I_{90} \propto MCS(M)_{90} \tag{7}$$

$$t \propto M^a C$$

where S_{90} is the structure factor at $\theta = 90°$ and a is a constant which depends on the structure of the particles. We will show below that for branched PMMA in THF $a = 0.4$. From relation 7 it is clear that I_{90} is most sensitive to large particles and that the sensitivity of t is intermediate between that of I_{90} and RI.

The q-dependence of I/C at different values of V_e is shown in Figure 3 for sample H. As expected, the q-dependence of I increases with decreasing V_e. $S(qR_g)$ can be obtained by plotting $I(q)/I(q=0)$ vs qR_g. If $S(qR_g)$ is independent of the size of the particles, all curves in Figure 3 superpose to form a master curve of $S(qR_g)$. Unfortunately, for the larger particles the experimental q-range is too small to allow a direct calculation of $I(q=0)$ and R_g using eq 2. In this case we can determine $I(q=0)$ and R_g from the shift factors needed to form a

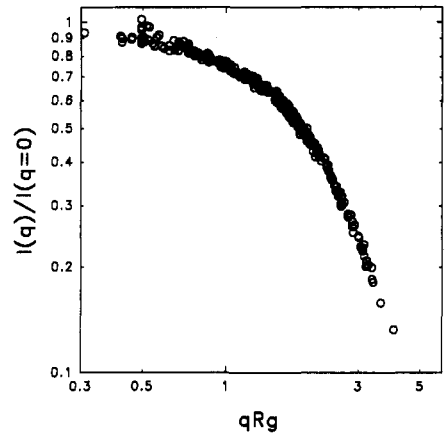

Figure 4. Master curve obtained by plotting $I(q)/I(q=0)$ versus qR_g; see text.

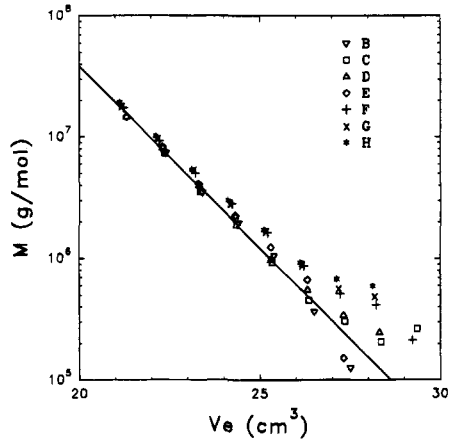

Figure 5. Semilogarithmic representation of M versus the elution volume of samples at different reaction extents (see Table 1). The solid line represents a linear least squares fit using only unbiased data.

master curve. Since we can determine the constant k independently, we can calculate M from $I(q=0)$ using eq 1. However, direct application of this method to the results shown in Figure 3 leads to unreasonably high values of R_g and M at larger values of V_e. The reason is that the scattered light intensity is modified by traces of very high molar mass particles which leave the column at larger elution volumes together with the normally eluted lower molar mass fractions. We have observed similar abnormal elution for a number of other systems that contain very large branched particles.[19] In order to determine an unbiased static structure factor, we have used for the smaller particles I/C values obtained from samples at lower reaction rates which did not contain these very high molar mass particles. A small part of samples E–H is fully excluded so that the fraction containing the largest molar masses is more polydisperse. However, for these very large particles, $qR_g \gg 1$ so that the effect of polydispersity on the particle structure factor is small. The master curve shown in Figure 4 was obtained by combining the results of a large number of independent experiments. The spread in the data gives a good idea of the precision of the method. In Figure 5 we have plotted M as a function of V_e for each sample on a semilogarithmic scale. It is clear that the deviation of M from the unbiased behavior at larger V_e increases with increasing reaction extent. The corresponding values of R_g and intrinsic viscosity ($[\eta] = t/(t_{THF}C)$, with t_{THF} the flow time of pure THF) as a function of V_e are shown in Figures

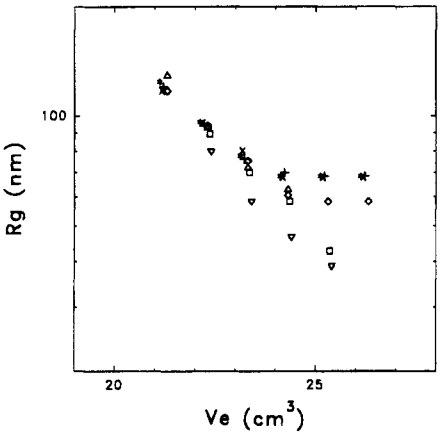

Figure 6. Semilogarithmic representation of R_g versus the elution volume of samples at different reaction extents. The symbols are the same as in Figure 5.

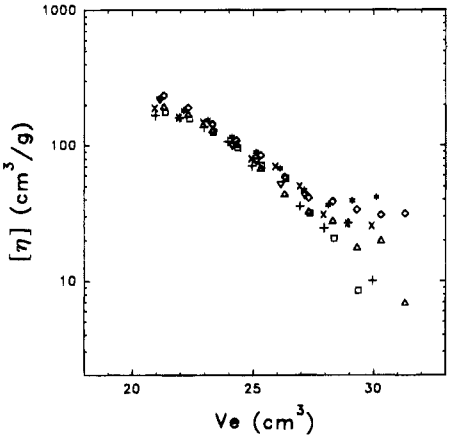

Figure 7. Semilogarithmic representation of $[\eta]$ versus the elution volume of samples at different reaction extents. The symbols are the same as in Figure 5.

6 and 7. As expected, the influence of traces of very large particles is more important for R_g which represents a z-average than for M which is a weight average. The influence on $[\eta]$, which is in between a number and a weight average, is even less. The influence on the RI signal, which is proportional to the concentration, is probably negligible.

Using the unbiased relation between M and V_e (solid line in Figure 5), we can plot $[\eta]$ and R_g as a function of M. Double-logarithmic representations of the results for the least biased fractions are shown in Figures 8 and 9. The data are compatible with a power law dependence of $[\eta]$ and R_g on M:

$$[\eta] = (0.285 \pm 0.02)M^{0.40\pm0.02}\ \text{cm}^3\cdot\text{g}^{-1}$$

$$R_g = (4.3 \pm 0.4) \times 10^{-2}M^{0.48\pm0.05}\ \text{nm} \qquad (8)$$

$([\eta]M)^{1/3}$ has the dimension of size and is for linear polymers related to R_g through the so-called[20] universal constant (Φ).

If we define a viscosity radius R_η as $(3[\eta]M/10\pi N)^{1/3}$, with N Avogadro's number, we obtain

$$R_\eta = (3.6 \pm 0.4) \times 10^{-2}M^{0.47\pm0.02}\ \text{nm} \qquad (9)$$

The ratio of the two radii is in good agreement with the value of Φ reported for linear PMMA.[21]

According to the universal calibration principle[13] (UC), the product $[\eta]M$ is the same at the same elution

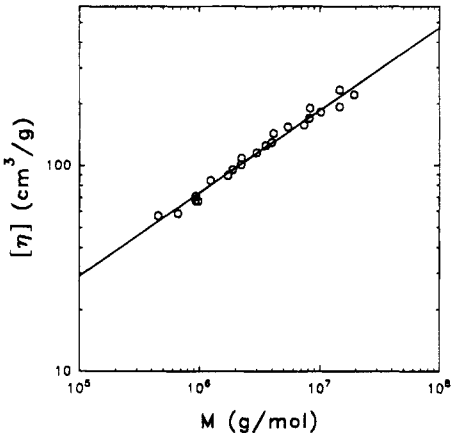

Figure 8. Double-logarithmic plot of $[\eta]$ versus M of the unbiased fractions. The solid line has a slope of 0.4.

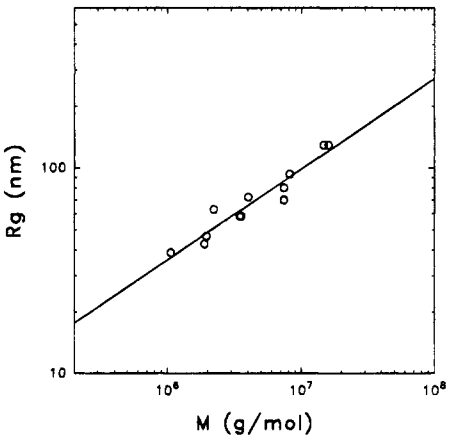

Figure 9. Double-logarithmic plot of R_g versus M of the unbiased fractions. The solid line has a slope of 0.48.

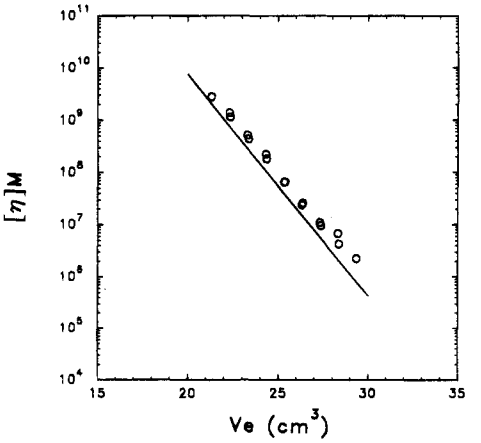

Figure 10. Comparison of $[\eta]M$ as a function of V_e for linear polystyrene (solid line) and branched PMMA (circles).

volume for different particles unless the structural architecture is very different. In Figure 10 we have plotted $[\eta]M$ as a function of V_e for branched PMMA and polystyrene standards. The polystyrene standards are systematically lower by about 25%. It is difficult to judge whether the difference between the values of $[\eta]M$ for the two systems is due to a systematic error in the determination of M or a deviation of UC. It is important to note, however, that we have used the weight-average molar mass and an average viscosity in between a weight and a number average. It is difficult to quantify the effect of using these averages as the precise shape of the band broadening is not known, but

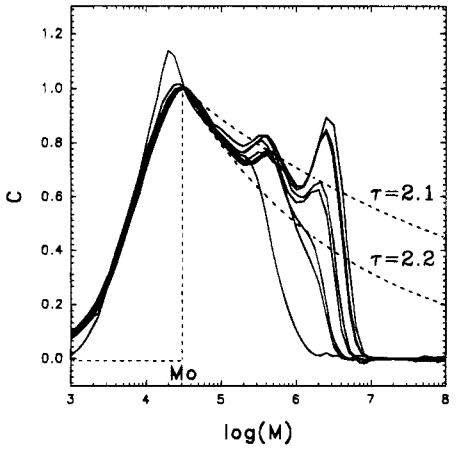

Figure 11. Comparison of the molar mass distributions of all samples with theoretical curves using eq 6 with τ equal to 2.1 and 2.2 and $M_0 = 3.2 \times 10^4$ g·mol^{-1} (dashed curves). The cutoff function was taken equal to unity.

it might explain the observed deviation.

In Figure 11 we have plotted the concentration as a function of log(M). In this semilogarithmic representation, C is proportional to $M^2N(M)$ so that, using eq 6, $C \propto M^{2-\tau}$ for $M_0 < M < M^*$. For $\tau < 2$ the maximum of C depends on M^* while for $\tau > 2$ the maximum is at $M = M_0$ independent of M^*. For the special case of $\tau = 2$, C is constant between M_0 and M^*. The solid lines in Figure 11 represent theoretical distributions with τ = 2.1 and 2.2, using $M_0 = 32\,000$ g·mol^{-1}. Of course, the real distribution does not have an abrupt cutoff at $M < M_0$ due to the polydispersity of the linear PMMA. For $M > M_0$ the overall shape of the distribution is well described by eq 6 with τ between 2.1 and 2.2. However, the experimental distribution contains undulations around the smooth distribution calculated from eq 6. As mentioned above, the upturn at the largest M can be explained by the limited resolution of the column, but we have at this stage no explanation for the deviation from a smooth distribution at intermediate values of M. We have observed similar undulations on broad distributions of branched polyurethane formed by polycondensation.[19] Such undulations have also been observed by Schosseler et al.[8] on broad distributions of branched polystyrene and by Patton et al.[7] in the case of branched polyesters. The undulations are either representative of the distribution or an artifact of SEC. The first option implies that during the polymerization certain sizes are formed by preference.

If we want to determine explicitly the cutoff function at M^* in eq 6, we are limited to those samples where even the largest particles in the distribution are well separated. We have chosen a stretched exponential form for cutoff function: $f(M/M^*) = \exp[-(M/M^*)^\beta]$. Large values of β give a sharp cutoff while smaller values give a more gradual cutoff. The experimental data show a rather sharp cutoff which is well described by a stretched exponential with $\beta = 3$ as shown in Figure 12 for sample B with $M^* = 2.6 \times 10^6$ g·mol^{-1} for $\tau = 2.2$ and $M^* = 2.4 \times 10^6$ g·mol^{-1} for $\tau = 2.1$.

The weight-average molar masses of all samples have been determined using the calibration curve shown in Figure 5 (M_{cal}) and are given in Table 1. These values can be compared with direct measurements of M_w of the polydisperse samples; see Table 1. M_{cal} of the higher molar mass samples is too small due to the limited resolution of the column.

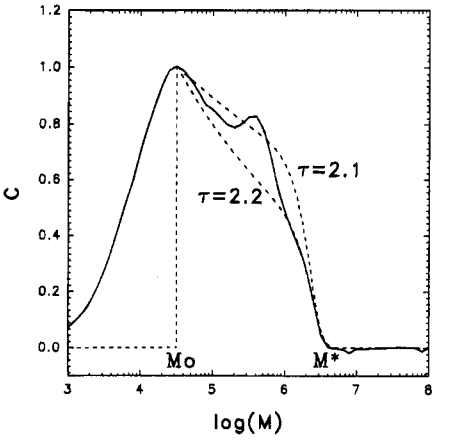

Figure 12. Comparison of the molar mass distribution of sample B with theoretical curves using eq 6 with τ equal to 2.1 and 2.2 and $M_0 = 3.2 \times 10^4$ g·mol^{-1} (dashed curves). A stretched exponential cutoff function was used with $\beta = 3$ and $M^* = 2.6 \times 10^6$ g·mol^{-1} for $\tau = 2.2$ and $\beta = 3$ and $M^* = 2.4 \times 10^6$ g·mol^{-1} for $\tau = 2.1$.

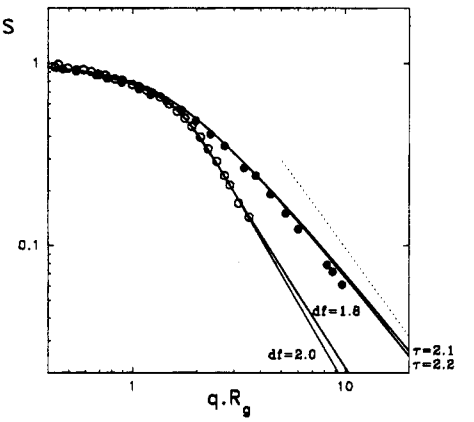

Figure 13. Comparison of the polydisperse (filled circles) and the monodisperse (open circles) static structure factor with theoretical curves (solid lines); see text. The dotted line has a slope of −1.6. For clarity, groups of data have been averaged at equal distance on a logarithmic scale.

Discussion

From eq 4 it follows that the q-dependence of I is influenced by polydispersity. It is therefore interesting to compare the static structure factor of the monodisperse fractions ($S(qR_g)$) with that of the polydisperse sample ($S(qR_{gz})$), which can be determined by plotting $I/I(q=0)$ versus qR_{gz}. The scattered light intensity was measured as a function of q for the polydisperse samples at different reaction rates. $S(qR_{gz})$ was determined by superposition in a way analogous to the determination of $S(qR_g)$. Results of a more detailed study of the polydisperse system using static and dynamic light scattering will be reported elsewhere. By definition, $S(qR_{gz})$ and $S(qR_g)$ are the same in the Guinier regime, but they clearly deviate at larger values of qR_{gz} or qR_g; see Figure 13. For clarity, we have averaged groups of data at equal distance on the logarithmic scale. Following Klein et al.,[1] we have fitted $S(qR_g)$ to an empirical equation which has the right behavior in the limits of low and high qR_g values

$$S(qR_g) = \left[1 + \frac{8}{3d_f}(qR_g)^2 + c_1(qR_g)^4 + c_2(qR_g)^6 + c_3(qR_g)^8\right]^{-d_f/8} \quad (10)$$

and contains three adjustable parameters (c_1 to c_3) to describe the shape at intermediate values of qR_g. A nonlinear least squares fits gives $d_f = 1.84$, $c_1 = 1.38$, $c_2 = -0.49$, and $c_3 = 0.114$. Unfortunately, the qR_g range is too small to determine d_f with high precision; e.g., fixing $d_f = 2$, which is close to the value obtained from the relation between M and R_g, gives an almost equally good fit (see Figure 13). However, we can exclude values of d_f lower than 1.7. For the polydisperse samples we are not limited by the resolution of the SEC so that we can measure samples with very large R_{gz}. In fact, for samples at different reaction extents close to the gel point we observe $I \propto q^{-1.6\pm0.03}$ over the whole accessible q-range from which we conclude that $d_{f,pol} = 1.6 \pm 0.03$. As we have seen above, d_f and $d_{f,pol}$ differ only if $\tau > 2$, in which case $d_{f,pol} = d_f(3 - \tau)$. The observed value of $d_{f,pol}$ implies that if $d_f = 1.8$ then $\tau = 2.1$ and if $d_f = 2.0$ then $\tau = 2.2$. Knowing $S(qR_g)$ and $N(M)$, we can calculate the z-average static structure factor of the polydisperse sample as

$$S_{poly} = \frac{\sum M^2 N(M) S(M)}{\sum M^2 N(M)} \qquad (11)$$

To calculate the static structure factor of a particle with mass M, we use the result of a fit to eq 10 to obtain $S(qR_g)$ and eq 3b to relate M to R_g. To calculate $N(M)$ we have used eq 6 with a stretched exponential cutoff function. We note that for the calculation of $S(qR_{gz})$ the prefactors in eqs 3b and 6 are unimportant. From SEC we know that τ is between 2.1 and 2.2 and β is about 3. In order to be consistent with the observed value for $d_{f,pol}$, we have calculated $S(qR_{gz})$ using two combinations of d_f and τ: $d_f = 2$ with $\tau = 2.2$ and $d_f = 1.8$ with $\tau = 2.1$. The results of these calculations are compared with the experimental data in Figure 13. The static structure factor of the polydisperse sample is well described using either of the two combinations. However, the final slope, indicated by the dotted line, is reached at lower qR_{gz} values than expected for the calculations.

It has been proposed that the aggregation of highly interpenetrated particles can be compared to a static percolation process.[22] Computer simulations of the percolation process show that fractal objects are formed with $d_f = 2.5$ with a mass distribution consistent with eq 6 using $\tau = 2.2$. If the system is diluted in a good solvent, it is expected that d_f is reduced by the effect of swelling due to excluded volume effects. Complete swelling would result in $d_f = 2.0$. The experimental results are consistent with these predictions except that we observe a much sharper cutoff of the mass distribution than found in the simulations.

Conclusions

(i) SEC in combination with multiangle light scattering is an excellent tool for the characterization of broad particle distributions. If the particles are self-similar, the static structure factor can be obtained by combination of the q-dependent light scattering intensities at different elution volumes. The application of the method is, however, limited by the quality of commercially available columns: the maximum size that can be effectively separated is about $R_g = 80$ nm and traces of very large particles ($R_g > 70$ nm) are eluted together with smaller particles at large V_e. It is clear that new types of column material need to be developed to allow a better SEC analysis of large particles.

(ii) The RI signal of broad distributions of branched polymers shows marked undulations. A more detailed study of this effect is needed to establish whether the undulations are representative of the distribution or an artifact of SEC.

(iii) A comparison of the static structure factor of the polydisperse sample with that of the monodisperse fractions can be used to determine the mass distribution if a wide enough range of qR_g and qR_{gz} is covered.

(iv) Application of the universal calibration to branched PMMA leads to 25% lower estimates of the molar mass than values obtained by light scattering measurements.

(v) The structure and mass distribution of particles formed by copolymerization of MMA and EGDMA are consistent with those obtained in a static percolation process.

References and Notes

(1) Klein, R.; Weitz, D. A.; Lin, M. Y., Lindsay, H. M.; Ball, R. C.; Meakin, P. *Prog. Colloid Polym. Sci.* **1990**, *81*, 161.
(2) Dietler, G.; Aubert, C.; Cannell, D. S.; Wiltzius, P. *Phys. Rev. Lett.* **1986**, *57*, 3117.
(3) Gimel, J.-C.; Durand, D.; Nicolai, T. *Macromolecules* **1994**, *27*, 583.
(4) Bouchaud, E.; Delsanti, M.; Adam, M.; Daoud, M.; Durand, D. *J. Phys. Fr.* **1986**, *47*, 1273.
(5) Wu, W.-L.; Bauer, B. J.; Su, W. *Polymer* **1989**, *30*, 1384.
(6) Fang, L.; Brown, W.; Konak, C. *Macromolecules* **1991**, *24*, 6839.
(7) Patton, E. V.; Wesson, J. A.; Rubinstein, M.; Wilson, J. C.; Oppenheimer, L. E. *Macromolecules* **1989**, *22*, 1946.
(8) Leibler, L.; Schosseler, F. *Phys. Rev. Lett.* **1985**, *55*, 1110. Schosseler, F.; Daoud, M.; Leibler, L. *J. Phys. Fr.* **1990**, *51*, 2373.
(9) Bauer, J.; Burchard, W. *Macromolecules* **1993**, *26*, 3103.
(10) Daoud, M.; Martin, J. E. In *The Fractal Approach to Heterogeneous Chemistry*; Aunir, D., Ed.; Wiley & Sons: Chichester, 1989.
(11) Vicsek, T. *Fractal Growth Phenomena*; World Scientific: London, 1989.
(12) Stauffer, D. *Introduction to Percolation Theory*, 2nd ed.; Taylor and Francis: London, 1992.
(13) Benoit, H.; Grubizic, Z.; Rempp, P.; Dekker, D.; Zilliox, J. G. *J. Chem. Phys.* **1966**, *63*, 1507.
(14) Huglin, J. B., Ed. *Light Scattering from Polymer Solutions*; Academic Press: London, New York, 1972.
(15) Yamakawa, H. *Modern Theory of Polymer Solutions*; Harper and Row: New York, 1971.
(16) Teixeira, J. In *On Growth and Forms*; Stanley, H. E., Ostrowsky, N., Eds.; Martinus Nijhoff Publishers: Dordrecht, 1986; pp 145–162.
(17) Nicolai, T.; Gimel, J.-C.; Durand, D. *Phys. Rev. B* **1995**, *51*, 11348.
(18) Busnel, J.-P.; Degoulet, C.; Nicolai, T.; Woodley, W., Patin, P. *J. Phys. III*, accepted.
(19) Degoulet, C. Thesis, 1994.
(20) Doi, M.; Edwards, S. F. *The Theory of Polymer Dynamics*; Clarendon Press: Oxford, 1986.
(21) Fujii, Y.; Tamai, Y.; Konishi, T.; Yamakawa, H. *Macromolecules* **1991**, *24*, 1608.
(22) de Gennes, P.-G. *Scaling Concepts in Polymer Physics*; Cornell University Press: London, 1979.

MA946368W